Journal Article (post-print version)

Performance Limits of THz Dispersive Spectroscopes Employing Super-Resolution Imaging

Robin Zatta, Ullrich R. Pfeiffer

This document is the accepted manuscript version that has been published in final form in:

IEEE Transactions on Terahertz Science and Technology
https://doi.org/10.1109/TTHZ.2021.3088278

© 2021 IEEE. Personal use of this material is permitted. Permission from IEEE must be obtained for all other uses, in any current or future media, including reprinting/republishing this material for advertising or promotional purposes, creating new collective works, for resale or redistribution to servers or lists, or reuse of any copyrighted component of this work in other works.

Persistent identifier of this version: https://doi.org/10.25926/k4nn-rz34

Universitätsbibliothek

BERGISCHE UNIVERSITÄT WUPPERTAL

This article has been accepted for publication in IEEE Transactions on Terahertz Science and Technology. This is the author's version which has not been fully edited and content may change prior to final publication. Citation information: DOI 10.1109/TTHZ.2021.3088278

Performance Limits of THz Dispersive Spectroscopes Employing Super-Resolution Imaging

Robin Zatta and Ullrich R. Pfeiffer *Fellow, IEEE*

***Abstract*—The performance of terahertz (THz) dispersive spectroscopes is limited in spectral resolution and frequency accuracy due to a finite pixel count. This paper demonstrates that increasing the synthetic effective pixel count by exploiting super-resolution (SR) imaging results in improved performance. To this end, we investigated the performance of a CMOS camera-based THz dispersive spectroscope using SR imaging. From 0.75–0.9 THz, average spectral resolution improved from 76 GHz to 34.2 GHz (about a factor of two), while the average frequency accuracy enhanced from 30 GHz to 1.65 GHz. Further to providing enhanced spectral resolution and frequency accuracy, our results provide an insight into the fundamental performance limits. For low-resolution (LR) imaging, the finite pixel count sets the spectral resolution limit, and for SR imaging, the camera angular resolution defines the limiting factor. For this reason, SR imaging generally improves the spectral resolution at least by a factor of two. Pixel count and noise fluctuation limit the frequency accuracy using LR and SR imaging, respectively.**

***Index Terms*—Terahertz (THz), spectroscope, spectrometer, CMOS, camera, spectral resolution, frequency accuracy.**

I. Introduction

TERAHERTZ spectroscopy describes the analysis of the interaction between matter and electromagnetic THz waves [1]–[3]. Many dielectric materials are transparent to THz radiation, like fabric, paper, cardboard, wood, masonry, plastic, and ceramic, being opaque to infrared or visible radiation [4]. THz spectroscopy, therefore, makes it possible to examine packaged goods for material properties. The whole process is non-destructive, as THz waves are non-ionizing because of low photon energy levels [4].

THz spectrometers are systems that combine a spectroscope with a matching broadband radiation source, thus allowing examining the material properties of matter. Established systems are THz time-domain spectrometers [5] and continuous-wave spectrometers [6], which are outstanding in terms of operating bandwidth, spectral resolution, and frequency accuracy. However, they are mostly not compatible with conventional microelectronics and only usable in laboratory environments because of their high manufacturing costs and low integration capabilities. This fact renders such devices unsuitable for mobile spectroscopy applications.

THz spectroscopy systems integrated into silicon process technologies have advantages in cost and integration complexity compared to the established THz spectrometers discussed above. Recent research indicates that silicon-based front-ends represent a low-cost alternative for high-precision spectroscopy applications. In particular, a SiGe-HBT transmitter with 4.1% bandwidth around 0.5 THz [7] and a SiGe-HBT sensor system with 4.5% bandwidth around 0.245 THz [8] have been presented. These systems were designed for low-pressure gas spectroscopy. This requires a high spectral resolution, while a narrow bandwidth is relatively unproblematic, at least for some applications. However, these systems lack the bandwidth requirements to characterize solids that exhibit broadband spectral masks. It is noted that such high spectral resolution as is required in gas spectroscopy is not necessary for the characterization of spectral masks of solids. Also, the narrow-bandwidth systems under discussion cannot perform free-space spectrum analysis of radiators, for example, to measure the higher harmonics of automotive radar chipsets to ensure compliance with electromagnetic interference (EMI) regulations. To clarify, spectral mask characterization of solids is attributed to spectrometers, whereas free-space spectrum analysis of radiators is attributed to spectroscopes. Because of required resonant LC impedance matching networks, it is impossible to develop coherently operated silicon-based spectroscopy systems operating from DC to, e.g., 1 THz. In addition to that, power amplification is not possible above the maximum oscillation frequency, f_{max}, of transistors. One approach to overcome such bandwidth limitations is the simultaneous operation of several harmonics [9]. In the cited work, multi-color imaging has been presented from 0.16–1.05 THz. However, full spectral coverage is not provided. For this reason, the given system is not capable of performing broadband spectroscopy. Instead, gaps in between these harmonics limit the applicability to multi-color imaging. Thus, there is currently no coherently operated spectroscopy system integrated into silicon process technologies suitable for characterizing the spectral masks of solids or the harmonic content of THz radiators.

Another approach to realize a THz spectrometer with silicon-based components is to map radiation of the broadband radiation source spatially on several antenna-coupled direct power detectors, representing an incoherent system approach. Since direct power detectors of THz radiation operate incoherently, they are not able to differentiate distinct frequencies. For this reason, each frequency must be mapped to a distinct spatial location, which is to say, a different detector. Toward realizing THz spectrometers, silicon-based spatially-mapped spectroscopes have been realized, such as SiGe-HBT on-chip spectroscopes based on a multi-mode antenna [10], [11] and our THz dispersive spectroscopes based on a CMOS camera [12], [13]. The one from [13] employs a mirror-type spectrograph (or monochromator). To clarify, a dispersive spectroscope combines a spectrograph (dispersive optics and several collimating optics)

The German Research Foundation supported this work under the individual grant project "Spatially-Mapped Mobile Terahertz Spectroscopy (T-MAP)." *(Corresponding author: Robin Zatta.)*

Robin Zatta and Ullrich R. Pfeiffer are with the Institute for High-Frequency and Communication Technology, University of Wuppertal 42119, Wuppertal, Germany (e-mail: zatta@uni-wuppertal.de, ullrich.pfeiffer@uni-wuppertal.de).

© 2021 IEEE. Personal use is permitted, but republication/redistribution requires IEEE permission. See https://www.ieee.org/publications/rights/index.html for more information.

This article has been accepted for publication in IEEE Transactions on Terahertz Science and Technology. This is the author's version which has not been fully edited and content may change prior to final publication. Citation information: DOI 10.1109/TTHZ.2021.3088278

with a camera. Briefly, the spectrograph projects radiation to a different angle of incidence of the camera and thus into a different camera pixel (or detector). Mirrors are superior to lenses in terms of signal propagation losses. Therefore, our spectroscope that employs a mirror-type spectrograph is superior to lens-based ones from [12], [14], [15] in terms of total efficiency of the spectrograph due to less severe signal propagation losses. Albeit multi-mode antenna-based spectroscopes represent single-chip solutions, they require significant calibration and post-processing to extract frequency information and act in the near-field, limiting the scope of practical applications. In comparison, CMOS camera-based ones are superior in simplicity and scalability, act in the far-field, and are implemented in cheaper technology. These advantages go hand in hand with a greater number of practical applications. One application represents the characterization of the harmonic content of radiators in free space, or, in other words, free-space spectrum analysis. Upgraded with a suitable broadband radiation source, such as that of [16], the characterization of spectral masks of solids can be addressed. It is noted that the CMOS detectors can be replaced by other direct power detectors, such as microbolometers [17], CMOS-NEMS [18], SiGe HBTs [19], and Schottky barrier diodes [20], provided that they can be integrated into a single chip.

Our previously published mirror-based THz dispersive spectroscope spans a bandwidth of several hundreds of GHz but exhibits only a moderate spectral resolution and frequency accuracy of several tens of GHz due to the limited pixel count [13]. This paper shows the fundamental spectroscope performance limits in terms of spectral resolution and frequency accuracy for the case where the number of pixels is not the limiting factor. To this end, SR imaging was employed to increase the synthetic effective pixel count, thereby reaching the camera angular resolution limit [21], [22]. We confirm that a larger pixel count, accompanied by enhanced angular resolution, improves the spectral resolution, in agreement with [23]–[25], as well as the frequency accuracy. Improved performance in these parameters is accompanied by better estimation of spectral masks of solids and harmonic content of radiators.

II. THz Dispersive Spectroscope

In [13], we have presented a THz dispersive spectroscope, realized by extending a CMOS camera with a custom-machined spectrograph. A conceptual system view of this spectroscope is illustrated in Fig. 1, which combines the spectrograph (mirror-based optical sub-system) with the CMOS THz camera. The spectrograph consists of two collimating mirrors and one reflective dispersive optic, and it projects each frequency of radiation emanating from a source to a different camera incidence angle. Thereafter, the camera lens maps radiation for each angle of incidence into a particular pixel. Consequently, beams scan along a given central pixel column with increasing source radiation frequency. To turn this spectroscope into a spectrometer, a THz source is required, and the mirror-based optical sub-system must be expanded, as indicated in the conceptual system view. Specifically, further collimating mirrors are required to focus the source beam on where the

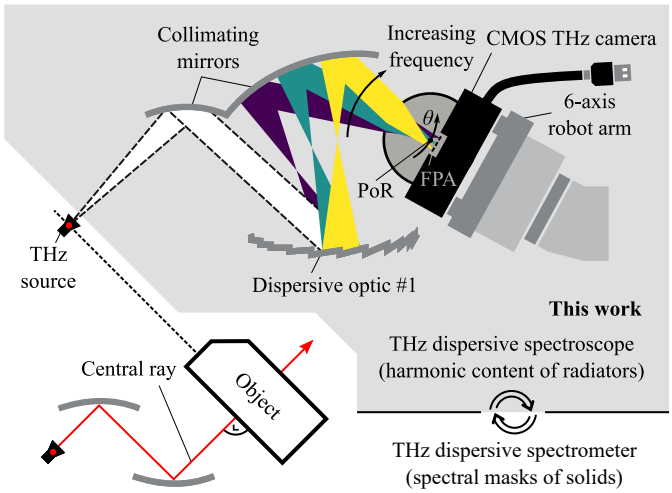

Figure 1. Conceptual system view of the mirror-based THz spectroscope using a CMOS camera and a dispersive optic. Here, the camera was mounted onto a 6-axis table-top robot arm to acquire images at angular offsets along θ. The camera lens center denotes the point of rotation (PoR). If one converts the spectroscope into a spectrometer, as illustrated, one can replace the source with an object, allowing characterizing its material properties. For this purpose, the mirror-type optical sub-system (spectrograph) must be extended by additional collimating mirrors that focus the source beam. For accurate measurements, a normal angle of incidence must be ensured for the central ray.

THz source situates in the spectroscope configuration. Creating a focal point is essential when inspecting an object in a spectrometer configuration. In that case, one wants to assure that all radiation passes through a material under a normal angle of incidence not to deflect radiation in another direction, which would cause a systematic error, effectively lowering the spectral resolution and frequency accuracy. Anyhow, the spectrometer is not of interest to this work. Instead, this work centers around the performance limits of the spectroscope in terms of spectral resolution and frequency accuracy. When turning the spectroscope into a spectrometer, both parameters would also be affected by source characteristics. These remain unconsidered in this work.

The modularity of the spectrograph allows covering different frequency bands. Two dispersive optics targeting different frequency bands were investigated previously. The following has been found. First, incident radiation frequency is recoverable over a ∼50% bandwidth. Hence, the two dispersive optics (#1 and #2) with design frequencies of 0.46 THz and 0.85 THz cover almost the entire 0.3–1.1 THz band. Second, the measured efficiency of the bespoke modular spectrograph is ∼75% only near the center frequencies of the dispersive optics but deteriorates away from this frequency, and third, spectral resolution and frequency accuracy are limited to several tens of GHz using LR imaging due to the finite pixel count.

This paper presents that SR imaging always results in maximum achievable spectral resolution and frequency accuracy. Because of signal-to-noise ratio (SNR) limitations concerned with spectroscope efficiency constraints, we concentrated our efforts on analyzing the spectroscope from 0.75–0.9 THz to ensure sufficient SNR for the most accurate measurements. In the following, theoretical spectral resolution and frequency accuracy limits using LR and SR imaging are discussed.

© 2021 IEEE. Personal use is permitted, but republication/redistribution requires IEEE permission. See https://www.ieee.org/publications/rights/index.html for more information.

This article has been accepted for publication in IEEE Transactions on Terahertz Science and Technology. This is the author's version which has not been fully edited and content may change prior to final publication. Citation information: DOI 10.1109/TTHZ.2021.3088278

A. Spectral Resolution

The spectral resolution of a THz dispersive spectroscope describes the maximum resolvable frequency difference for two simultaneously incident frequencies. Suppose the pixel count is the limiting factor, as in LR imaging. In that case, the number of spectral peaks the spectroscope can resolve, $N_{\mathrm{Peaks,resolvable}}$, equals half the number of pixels, N_{Pixels}, into which radiation of incident frequencies is mapped:

$$N_{\mathrm{Peaks,resolvable}} = \frac{N_{\mathrm{Pixels}}}{2}. \tag{1}$$

Essentially, this is because one pixel is always required between two further ones to identify a discernible dip of an incident two-tone signal, as illustrated in Fig. 2(a) and (b). Consequently, for LR imaging, the average spectral resolution, $\delta\overline{f}$, is

$$\delta\overline{f} = \frac{BW}{N_{\mathrm{Peaks,resolvable}}} = 2 \cdot \frac{BW}{N_{\mathrm{Pixels}}}, \tag{2}$$

where BW is the system (or sub-system) bandwidth, and N_{Pixels} stands for the pixel count into which this bandwidth is mapped. An average spectral resolution is considered since the spectral-spatial mapping through the spectrograph may be nonlinear, as is the case with the spectroscope tested here [12]. Suppose the pixel count is not the limiting factor, as in SR imaging. Then, the spectral resolution limit discussed concerning LR imaging above can be overcome [Fig. 2(c) and (d)]. According to (2), the spectral resolution should become infinitely small for an infinite pixel count. However, this cannot be. In that case, the Rayleigh resolution comes into play. It is applicable for a spectroscope of this sort because spatially-mapped incident frequencies can be seen as distinct light sources. Hence, if the pixel count is no longer the limiting factor, the angular resolution of the camera limits the spectral resolution, and (2) modifies to:

$$\delta\overline{f} = \frac{BW}{N_{\mathrm{Pixels}}}. \tag{3}$$

When using SR imaging for an increased pixel count, the average spectral resolution becomes the average pixel bandwidth, or, in other words, the frequency-dependent spectral resolution becomes the frequency-dependent pixel bandwidth. In first-order approximation, the pixel bandwidth represents the spectral definition of the angular resolution of a pixel. This is not entirely correct because each pixel receives a range of frequencies, and the angular resolution of a pixel is frequency-dependent. The associated error, however, should be neglectable. Thus, SR imaging should improve the spectral resolution by a factor of two compared with LR imaging, as long as the angular resolution of the spectrograph is equally good or better than the camera angular resolution. Since the spectrograph provides collimated beams, this assumption can be made. Accordingly, the camera angular resolution should represent the limiting factor for the spectral resolution of the spectroscope. According to [21], the angular resolution of the camera is determined by the pixel half-power beamwidth (HPBW), therefore being the metric to consider for determining the spectral resolution of the spectroscope. The HPBW, which relates to directivity, is a 2-D function of frequency and off-axis displacement of the pixels [26]. Therefore, the spectral resolution limit should vary with frequency. In addition, the nonlinearity of the spatial–spectral mapping by the spectrograph, as described in [13], plays a role in the frequency dependence of the spectral resolution. For these reasons, the comparison between average spectral resolution and average pixel bandwidth for a given frequency range gives a good indication of the improvement in overall spectral resolution through SR imaging, which is to say, when the pixel count does not represent the limiting factor.

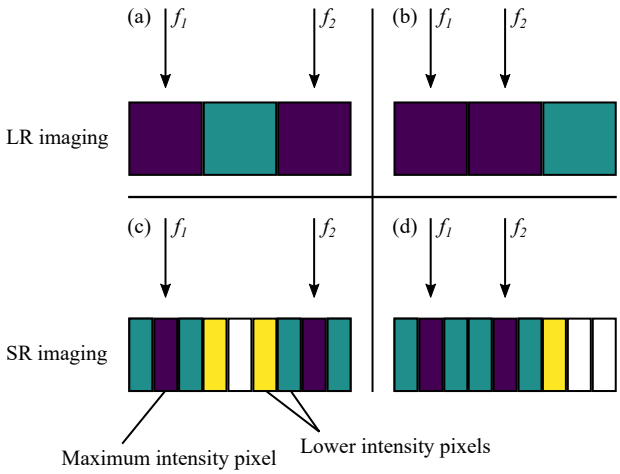

Figure 2. The reasoning for the enhancement in spectral resolution and frequency accuracy by employing SR imaging. In (a), radiation of two incident frequencies, f_1 and f_2, excites two pixels that a third one separates. In that case, f_1 and f_2 are resolved, and SR imaging can only improve the frequency accuracy associated with the maximum intensity pixels, as indicated in (c). In (b), f_1 and f_2 exciting two adjacent pixels are unresolved, and SR imaging can improve the spectral resolution, besides the frequency accuracy, as indicated in (d).

B. Frequency Accuracy

The frequency accuracy represents the offset of the measured frequency from the actual one. In the spectroscope, it is associated with the maximum intensity pixel, as indicated in 2(c). To clarify, maximum intensity pixel means the signal that receives the biggest portion of an incident radiation wavefront. Since that pixel defines the frequency accuracy, the frequency accuracy is also limited by a finite number of pixels, like the spectral resolution, as indicated in 2. Therefore, synthetically boosting the pixel count by SR imaging also improves the frequency accuracy. This applies to cases where LR imaging entails spectrally-resolved incident frequencies [Fig. 2(a) versus Fig. 2(c)] and where it does not [Fig. 2(b) versus Fig. 2(d)]. For LR imaging, the limit of average frequency accuracy should be approximately equal to the average pixel bandwidth. For SR imaging, there is no real limit for the frequency accuracy. Ultimately, however, the frequency accuracy is limited by an interaction of various noise sources. These noise sources include pixel noise, measurement alignment inaccuracy, and the surface tolerances of the camera lens and spectrograph.

III. Super-Resolution Imaging Method

Geometrical SR imaging is a class of widely used techniques to increase the pixel count of a camera by subpixel shifting. According to the discussions about the theoretical limits of

© 2021 IEEE. Personal use is permitted, but republication/redistribution requires IEEE permission. See https://www.ieee.org/publications/rights/index.html for more information.

This article has been accepted for publication in IEEE Transactions on Terahertz Science and Technology. This is the author's version which has not been fully edited and content may change prior to final publication. Citation information: DOI 10.1109/TTHZ.2021.3088278

spectral resolution, increasing the number of pixels means better spectral resolution and better frequency accuracy for the spectroscope. In addition to increased pixel count, such SR imaging methods can help achieve the diffraction-limited angular resolution given by the camera lens when beam separation is greater than the beam divergence. In other words, geometrical SR imaging overcomes the geometrical angular resolution limit given by the beam separation angle between adjacent pixels. Singleframe and multiframe methods are suitable for this purpose, both of which work on the principle of subpixel shifting. As the terminologies imply, the former performs subpixel shifting based on a single frame, while the latter uses multiple frames. We used a technique based on acquiring multiple LR images or, more specifically, 1-D LR vectors in this work. Acquiring 1-D vectors is sufficient for this work because it is unnecessary to probe all 1024 pixels, as the frequency-dependent incident beams scan horizontally along a given central pixel column [12]. Therefore, a simplified version of the geometrical multiframe SR technique from [22] was used. In contrast, the entire FPA was employed the cited work. Fig. 3(a) illustrates the subpixel shifting method we used. This illustration is an example based on three 1-D LR vectors. A superimposed 1-D SR vector with an increased pixel count and enhanced angular resolution is generated through subpixel shifting of these 1-D LR vectors. The whole process is scalable, and the pixel count of the 1-D SR vector is determined by the number of pixels situated in a pixel column of the camera and the number of 1-D LR vectors acquired. More generally, the 1-D SR vector can be described as

$$SR = \left(LR_{0,0}, LR_{0,1}, LR_{1,0}, LR_{1,1} \quad \dots \quad LR_{\mathrm{I},\Theta}\right), \quad (4)$$

where $LR_{\mathrm{i},\theta}$ contains information of a single camera pixel with the pixel #, i, situated in a given pixel column at a certain predictable angular position, θ. Subpixel shifting is realized by rotating around the camera lens center. As illustrated in Fig. 3(b), rotation around the camera lens center is accompanied by moving along the FPA. In effect, this is equivalent to performing a radiation pattern scan for each pixel. However, this radiation pattern scan is limited to a small angular range; specifically, to the beam separation angle between adjacent camera pixels. This way, an optimal sampling is ensured since far-field beams of adjacent pixels overlap at or above their individual full-width at half-maximum (FWHM) beam divergence angle, which is reflected in superimposed SR 1-D vectors. Besides an enhanced angular resolution, SR imaging is accompanied by an improved SNR. To clarify, in imaging, the SNR is described as the ratio of signal power to RMS image noise. The signal power increases due to acquiring multiple images, while the RMS image noise remains constant. Consequently, the SNR increases. This is valid in under- and oversampling cases. According to [22], the camera undersamples its FoV in the frequency range of interest for this work (0.75–0.9 THz) because beam separation between adjacent pixels is larger than the beam divergence. The SNR improvement is even more pronounced for frequencies at which the camera undersamples its FoV. When under-sampling, there are gaps in the camera FoV that are not sampled in those cases because there are radiation-insensitive areas between the camera pixels. SR imaging for oversampling can fill these gaps in the FoV since the rotation causes the previously unseen portions of an incident radiation wavefront to move to radiation-sensitive areas of the FPA. In summary, SR imaging improves the spectroscope performance in terms of spectral resolution and frequency accuracy of the spectroscope, and as a nice side effect, it increases the SNR beyond that.

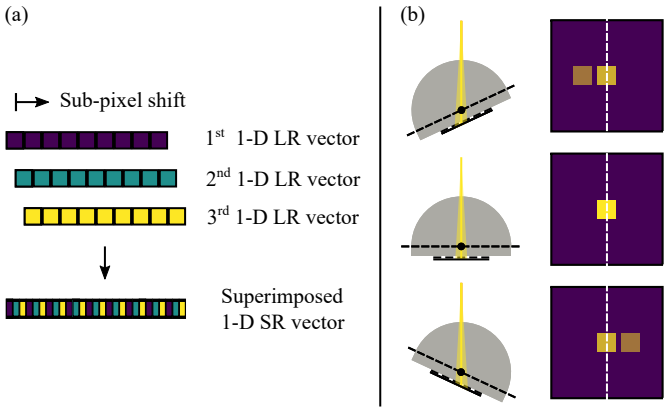

Figure 3. (a) Illustration of the geometrical multiframe SR algorithm used in this work. Several 1-D LR vectors acquired at angular offsets are combined into a 1-D SR vector through sub-pixel shifting. (b) Illustration of the measurement procedure to acquire multiple LR images or 1-D LR vectors at angular offsets. Rotation around the camera lens center causes incident radiation to move along the FPA. Specifically, incident radiation for a fixed frequency goes through three different scenarios from spreading across two adjacent pixels over focussing into the right of these two pixels to spread across this pixel and the next adjacent pixel, as indicated.

IV. Experiment and Measured Results

The experimental set-up to analyze the spectral resolution and frequency accuracy limits of the spectroscope is essentially the conceptual view of the spectroscope [Fig. 1(a)]. A continuous-wave 0.75–0.9 THz radiation source equipped with a 24.9–26.5 dBi standard gain horn antenna was employed. In the frequency range of interest, the radiation power of the source ranges between 0.5 μW and 8.8 μW, and integrated video-rate (30 fps) NEP of the camera and efficiency of the spectrograph (dispersive optic #1) range between 17.6 nW and 36.2 nW [27] and 24.3% and 71.1% [13], respectively. In order to realize a peak SNR above 30 dB for all source operating frequencies from 0.75–0.9 THz, frame-averaging of 1024 frames was applied. This improved the NEP of the camera by $\sqrt{1024}$, according to [28], i.e., to values ranging between 550 pW and 1.13 nW. The camera was mounted onto a 6-axis table-top UR5 robot arm for rotation. Multiple measurements were performed at each source operating frequency at angular offsets with the camera. Only a central pixel column was selected. It is unnecessary to probe all 1024 pixels, as the frequency-dependent incident beams scan horizontally along a given central pixel column [12]. With a polar raster scanning along θ, 22 LR 1-D vectors were acquired within 1.6° angular range ($\equiv$ beam separation angle between two adjacent pixels). Thus, the step size was 1.6°/22. The measurement took 75 minutes. LR data were processed according to (4). As a result, SR 1-D vectors with increased pixel count (704 subpixels) and

© 2021 IEEE. Personal use is permitted, but republication/redistribution requires IEEE permission. See https://www.ieee.org/publications/rights/index.html for more information.

This article has been accepted for publication in IEEE Transactions on Terahertz Science and Technology. This is the author's version which has not been fully edited and content may change prior to final publication. Citation information: DOI 10.1109/TTHZ.2021.3088278

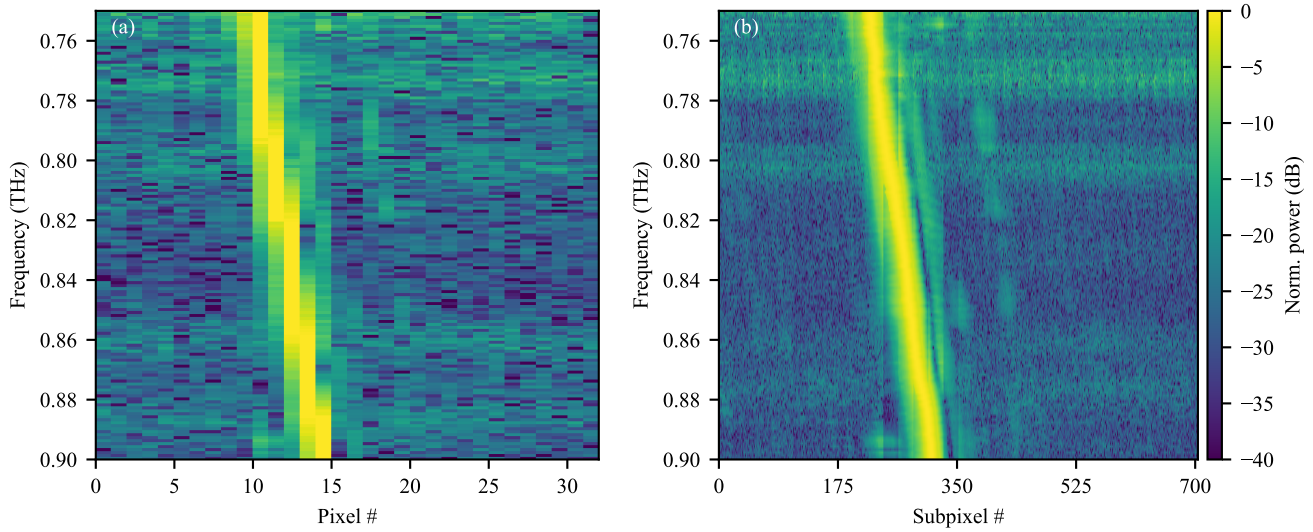

Figure 4. Normalized power as a 2-D function of frequency and pixel # and subpixel # using LR (a) and SR (b) imaging, respectively. Normalization is performed with respect to the maximum value obtained for each frequency. Crosses indicate the pixel crossovers.

an enhanced angular resolution were generated, leading to improved spectral resolution and frequency accuracy, as will be elaborated in the following.

Fig. 4(a) and (b) show the normalized power as a 2-D function of frequency and pixel # and subpixel # using LR and SR imaging, respectively. Varying peak SNR is characterized by higher noise in these normalized figures, leading to horizontally increased normalized power. As can be visually observed, SR imaging allows identifying more spectral features. The reason for this is twofold: on one hand, SR imaging enhances the angular resolution, and on the other hand, it increases the SNR. The few vertical streaks observed in the spectral SR image are due to pixel responsivity variation.

Fig. 5(a) shows the frequency-dependent spectral resolution plotted along with the frequency-dependent pixel bandwidth. The spectral resolution was obtained from frequency-dependent normalized 1-D SR vectors. Such vectors were normalized, as in [13], to make the spectral resolution determination independent of frequency-dependent spectroscope sensitivity and source radiation power. The spectral resolution was determined using the FWHM criterion, commonly used [29] and being close to Rayleigh's criterion, not applicable here because of single-tone excitation. More specifically, the spectral resolution was determined as the frequency difference for which spatially-mapped radiation for two incident frequencies overlap below their individual FWHM, evaluated as a function of the frequency. This procedure is similar to increasing the distance between two point sources until they are distinguishable, according to the FWHM criterion. This criterion represents a criterion usually associated with the resolution of spatially separated light sources. To clarify, for a dispersive spectroscope, it is applicable because the radiation of frequencies is spatially mapped, and each frequency can be considered a distinct light source. The pixel bandwidth was determined as the frequency range for which the detected signal is larger than the FWHM from normalized frequency-dependent pixel readouts. Here, normalization also includes calibrating for frequency-dependent TX radiation power. Since we also have calibrated for this, the pixel bandwidth gives us the angular resolution of a pixel under investigation, assuming that spatially-mapped radiation of incident frequencies is perfectly collimated. As explained earlier, two times the pixel bandwidth represents the spectral resolution limit for LR imaging because one pixel is required between two further ones to identify a dip between spatially overlapping radiation of two frequencies. As can be seen, SR imaging allows reaching an average spectral resolution about as low as the average pixel bandwidth, namely 35.17 GHz; the average pixel bandwidth is 34.15 GHz. Average spectral resolution was calculated by averaging all spectral resolution values from Fig. 5(a). Average pixel bandwidth was calculated by averaging the three values of pixel bandwidth from this figure. Thus, we have experimentally confirmed that SR imaging improves the average spectral resolution at least by a factor of two compared with using LR imaging [13]. Finally, the factor that limits the spectral resolution using SR imaging is clear. It is the pixel bandwidth of the spectroscope or, in other words, the angular resolution of the camera. It is noted that the spectral resolution fluctuates. Specifically, it varies within an RMS deviation of 5.95 GHz. Nevertheless, a similar trend is observed from inspection of the pixel bandwidth. Pixel-to-pixel crossovers (Fig. 4) may explain the wavelike trend of the spectral resolution. In effect, the pixel bandwidth relates to the angular resolution of the camera pixels, which in turn relates to the pixel directivity. Directivity depends upon both frequency and off-axis displacement to the lens center [26]. Therefore, pixel bandwidth and thus spectral resolution are frequency-dependent.

Fig. 5(b) shows maximum intensity pixel #-to-frequency and maximum intensity subpixel #-to-frequency mapping using LR and SR imaging, respectively. From this, we determined

© 2021 IEEE. Personal use is permitted, but republication/redistribution requires IEEE permission. See https://www.ieee.org/publications/rights/index.html for more information.

This article has been accepted for publication in IEEE Transactions on Terahertz Science and Technology. This is the author's version which has not been fully edited and content may change prior to final publication. Citation information: DOI 10.1109/TTHZ.2021.3088278

Table I
SILICON-BASED THZ SEPCTROSCOPY SYSTEMS

Reference	Technology	Operating bandwidth (THz)	Average spectral resolution (GHz)	Average frequency accuracy (GHz)	DC power consumption (mW)
[7]	0.13-µm SiGe	0.238–0.245	0.00138	$\leq$0.00138	1,467
[8]	0.13-µm SiGe	0.494–0.5	0.0005	$\leq$0.0005	1,100
[9]	0.25-µm SiGe BiCMOS	0.16–1.05[a]	-	-	600
[10]	0.13-µm SiGe BiCMOS	0.04–0.33	0.01	$\leq$0.01	212
[11]	0.13-µm SiGe BiCMOS	0.04–0.99	0.01[b]	0.01	212
[13]	65-nm CMOS	0.6–1.1[c]	84[d]	30[e]	0.035[f]
This work	**65-nm CMOS**	**0.75–0.9**[c,g]	**34.2**[h]	**1.65**	**0.035**[f]

[a] divided into six sub-bands; [b] predicted; [c] modularity of the dispersive optic can be leveraged to increase the operating bandwidth; [d] using two times pixel bandwidth criterion; [e] provided in this work; [f] 14 pixels probed to cover 0.6–1.1 THz and based on DC power consumption per pixel from [30]; [g] tested; [h] from 0.6–1.1 THz using one times pixel bandwidth 42 GHz based on outcomes of this work

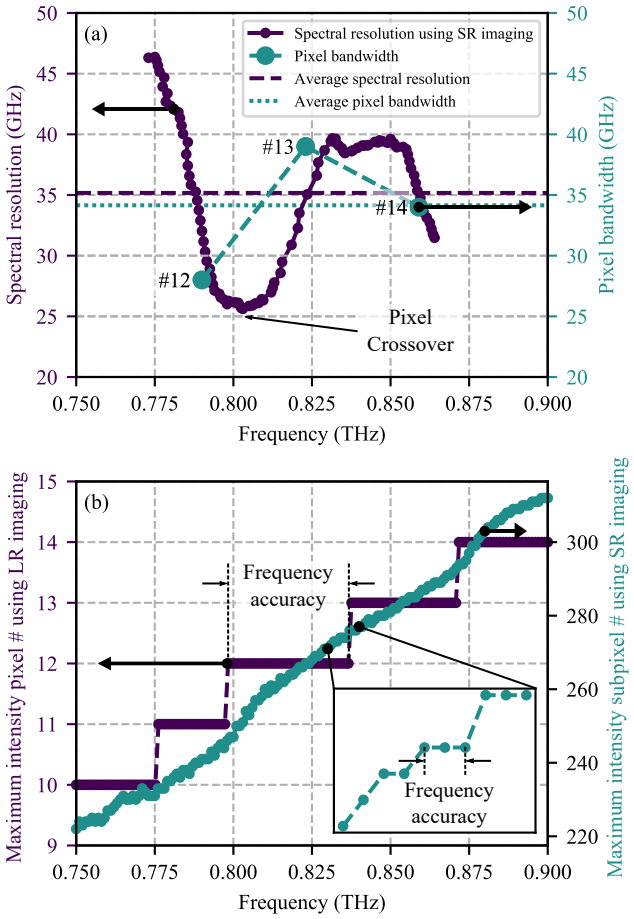

Figure 5. (a) Spectral resolution using SR imaging compared with pixel bandwidth. (b) Maximum intensity pixel # and subpixel # to frequency mapping using LR and SR imaging, respectively.

the frequency accuracy as the frequency step size for which a monotonically increasing pixel #-to-frequency mapping and subpixel #-to-frequency mapping holds using LR [example in Fig. 5(b)] and SR imaging, respectively. Since the scatter points that refer to SR imaging are pretty dense, a zoomed-in view giving an example for improved frequency accuracy is provided. The average frequency accuracy achieved is 30 GHz and 1.65 GHz using LR and SR imaging, respectively. In each case, the average values represent an average over "the width of all steps of the staircase measured in frequency" shown in Fig. 5(b). Hence, SR imaging is superior to LR imaging in terms of frequency accuracy by a factor of 18.2. This factor is close to the number of steps of the rotational scan of 22. Pixel noise, measurement alignment inaccuracy, and the surface tolerances of the camera lens and spectrograph are factors that prevent us from reaching the theoretical maximum improvement of 22. There is a small negative correlation of 14.9% between frequency-dependent peak SNR and frequency accuracy using SR imaging. Thus, the peak SNR achieved (30 dB) is sufficient for reaching high frequency accuracy.

In Table I, the herein achieved performance is compared with the performance of state-of-the-art silicon-based THz spectroscopy systems. In comparison to [13], the herein achieved average spectral resolution is two times better, and the frequency accuracy improved from 30 GHz to 1.65 GHz. Our SR imaging-based THz dispersive spectroscopy approach facilitates a convenient means to extract frequency information with high spectral resolution and frequency accuracy.

V. CONCLUSION

The performance of a state-of-the-art THz CMOS camera-based dispersive spectroscope from [13] has been enhanced in spectral resolution and frequency accuracy. Improvements were achieved by exploiting SR imaging. By boosting the synthetic effective pixel count and reaching the camera angular resolution limit, the spectral resolution was improved from 68.3 GHz to 34.2 GHz, whereas the frequency accuracy was increased from 30 GHz to 1.65 GHz. This work presents the best spectral resolution and frequency accuracy performance achieved with such THz spectroscopes.

SR imaging will be of general utility as a technique to effect maximum achievable spectral resolution and frequency accuracy using a THz dispersive spectroscope, with a minimum spectral resolution improvement by a factor of two and substantially better frequency accuracy. For fixed dimensions of the camera FPA, a larger lens is accompanied by better angular resolution and smaller FoV. Hence, a performance trade-off between spectral resolution, frequency accuracy, and operating bandwidth exists related to the camera lens choice.

In combination with [31], a CMOS camera would be capable of characterizing all far-field characteristics of THz sources, such as far-field radiation pattern, directivity, half-power beamwidth, radiation power, and harmonic content. The last two parameters are ascribed to the spectroscope. However,

© 2021 IEEE. Personal use is permitted, but republication/redistribution requires IEEE permission. See https://www.ieee.org/publications/rights/index.html for more information.

This article has been accepted for publication in IEEE Transactions on Terahertz Science and Technology. This is the author's version which has not been fully edited and content may change prior to final publication. Citation information: DOI 10.1109/TTHZ.2021.3088278

it should be noted that an equalization scheme for relative power measurements would be required to use the spectroscope to determine the power radiated at the various harmonics. Such an equalization scheme would also be required if turning the spectroscope into a spectrometer to perform relative power measurements for an object under test. For this purpose, the total efficiency from [13] can be used.

ACKNOWLEDGMENT

The authors would like to thank Ticwave GmbH, Wuppertal, Germany, for providing the CMOS THz camera. Also, they would like to thank Daniel Headland from the Osaka University, Osaka, Japan, and Philipp Hillger from the University of Wuppertal, Wuppertal, Germany, for their earlier contributions to realizing the herein investigated THz dispersive spectroscope.

REFERENCES

[1] M. C. Beard, G. M. Turner, and C. A. Schmuttenmaer, "Terahertz spectroscopy," 2002.
[2] J. B. Baxter and G. W. Guglietta, "Terahertz spectroscopy," *Anal. Chem.*, vol. 83, no. 12, pp. 4342–4368, 2011.
[3] S. L. Dexheimer, *Terahertz spectroscopy: principles and applications*. CRC press, 2017.
[4] R. E. Miles, X.-C. Zhang, H. Eisele, and A. Krotkus, *Terahertz frequency detection and identification of materials and objects*. Springer Science & Business Media, 2007.
[5] M. Van Exter, C. Fattinger, and D. Grischkowsky, "Terahertz time-domain spectroscopy of water vapor," *Opt. Lett.*, vol. 14, no. 20, pp. 1128–1130, 1989.
[6] A. Roggenbuck *et al.*, "Coherent broadband continuous-wave terahertz spectroscopy on solid-state samples," *New J. Phys.*, vol. 12, no. 4, 2010.
[7] K. Schmalz, J. Borngräber, W. Debski, P. Neumaier, R. Wang, and H. Hübers, "Tunable 500 GHz transmitter array in SiGe technology for gas spectroscopy," *Electron. Lett.*, vol. 51, no. 3, pp. 257–259, 2015.
[8] K. Schmalz, J. Borngräber, W. Debski, M. Elkhouly, R. Wang, P. F. . Neumaier, D. Kissinger, and H. Hübers, "245-GHz Transmitter Array in SiGe BiCMOS for Gas Spectroscopy," *IEEE Trans. Terahertz Sci. Technol.*, vol. 6, no. 2, pp. 318–327, 2016.
[9] K. Statnikov, J. Grzyb, B. Heinemann, and U. R. Pfeiffer, "160-GHz to 1-THz multi-color active imaging with a lens-coupled SiGe HBT chipset," *IEEE Trans. Microw. Theory Techn.*, vol. 63, no. 2, pp. 520–532, 2015.
[10] X. Wu and K. Sengupta, "On-Chip THz Spectroscope Exploiting Electromagnetic Scattering With Multi-Port Antenna," *IEEE J. Solid-State Circuits*, vol. 51, no. 12, pp. 3049–3062, 2016.
[11] X. Wu and K. Sengupta, "Single-chip source-free terahertz spectroscope across 0.04–0.99 THz: combining sub-wavelength near-field sensing and regression analysis," *Opt. Express*, vol. 26, no. 6, pp. 7163–7175, 2018.
[12] D. Headland, P. Hillger, R. Zatta, and U. Pfeiffer, "Incoherent, spatially-mapped THz spectral analysis," in *Proc. Int. Conf. Infrared Millim. Terahertz Waves*, 2018, pp. 1–2.
[13] D. Headland, R. Zatta, P. Hillger, and U. R. Pfeiffer, "Terahertz spectroscope using CMOS camera and dispersive optics," *IEEE Trans. Terahertz Sci. Technol.*, pp. 1–1, 2020.
[14] R. Eichholz, H. Richter, S. Pavlov, M. Wienold, L. Schrottke, R. Hey, H. Grahn, and H.-W. Hübers, "Multi-channel terahertz grating spectrometer with quantum-cascade laser and microbolometer array," *Appl. Phys. Lett.*, vol. 99, no. 14, p. 141112, 2011.
[15] N. Kanda, K. Konishi, N. Nemoto, K. Midorikawa, and M. Kuwata-Gonokami, "Real-time broadband terahertz spectroscopic imaging by using a high-sensitivity terahertz camera," *Sci. Rep.*, vol. 7, p. 42540, 2017.
[16] M. M. Assefzadeh and A. Babakhani, "Broadband Oscillator-Free THz Pulse Generation and Radiation Based on Direct Digital-to-Impulse Architecture," *IEEE J. Solid-State Circuits*, vol. 52, no. 11, pp. 2905–2919, Nov 2017.
[17] L. E. Marchese, M. Terroux, M. Bolduc, M. Cantin, O. Martin, N. Desnoyers, and A. Bergeron, "A 0.1 Megapixel THz camera with 17 degree field of view for large area single shot imaging," in *Proc. Int. Conf. Infrared Millim. Terahertz Waves*, 2014, pp. 1–2.
[18] D. Corcos, N. Kaminski, E. Shumaker, O. Markish, D. Elad, T. Morf, U. Drechsler, W. T. Silatsa Saha, L. Kull, K. Wood, U. R. Pfeiffer, and J. Grzyb, "Antenna-Coupled MOSFET Bolometers for Uncooled THz Sensing 0," *IEEE Trans. Terahertz Sci. Technol.*, vol. 5, no. 6, pp. 902–913, 2015.
[19] R. Al Hadi, J. Grzyb, B. Heinemann, and U. R. Pfeiffer, "A Terahertz Detector Array in a SiGe HBT Technology," *IEEE J. Solid-State Circuits*, vol. 48, no. 9, pp. 2002–2010, 2013.
[20] R. Han, Y. Zhang, Y. Kim, D. Y. Kim, H. Shichijo, E. Afshari, and K. K. O, "Active Terahertz Imaging Using Schottky Diodes in CMOS: Array and 860-GHz Pixel," *IEEE J. Solid-State Circuits*, vol. 48, no. 10, pp. 2296–2308, 2013.
[21] R. Zatta, R. Jain, J. Grzyb, and U. R. Pfeiffer, "Resolution Limits in Lens-Integrated CMOS THz Cameras Employing Super-Resolution Imaging," in *Proc. Int. Conf. Infrared Millim. Terahertz Waves*, Sep. 2019, pp. 1–2.
[22] R. Zatta, R. Jain, J. Grzyb, and U. R. Pfeiffer, "Resolution Limits of Hyper-Hemispherical Silicon Lens-Integrated THz Cameras Employing Geometrical Multiframe Super-Resolution Imaging," *IEEE Trans. Terahertz Sci. Technol.*, vol. 11, no. 3, pp. 277–286, 2021.
[23] Y. Zhang, K.-H. Song, B. Dong, J. L. Davis, G. Shao, C. Sun, and H. F. Zhang, "Multicolor super-resolution imaging using spectroscopic single-molecule localization microscopy with optimal spectral dispersion," vol. 58, no. 9, pp. 2248–2255, 2019.
[24] K. Kitano, T. Funatomi, R. Yasukuni, K. Tanaka, H. Kubo, Y. Hosokawa, and Y. Mukaigawa, "Super-resolution for a dispersive spectrometer using a tilted area sensor and spectrally varying blur kernel interpolation," *Opt. Express*, vol. 29, no. 2, pp. 2809–2818, 2021.
[25] A. Watanabe and H. Furukawa, "Super-resolution technique for high-resolution multichannel fourier transform spectrometer," *Opt. Express*, vol. 26, no. 21, pp. 27 787–27 797, 2018.
[26] D. F. Filipovic, G. P. Gauthier, S. Raman, and G. M. Rebeiz, "Off-axis properties of silicon and quartz dielectric lens antennas," *IEEE Trans. Antennas Propag.*, vol. 45, no. 5, pp. 760–766, 1997.
[27] V. S. Jagtap, R. Zatta, J. Grzyb, and U. R. Pfeiffer, "Performance Characterization Method of Broadband Terahertz Video Cameras," in *Proc. Int. Conf. Infrared Millim. Terahertz Waves*, Sep. 2019, pp. 1–2.
[28] R. Zatta *et al.*, "Characterization of the noise behavior in lens-integrated CMOS terahertz video cameras," *Terahertz Sci. Techn.—Int. J. THz*, vol. 11, no. 4, pp. 102–123, Dec. 2018.
[29] J. Demmerle, E. Wegel, L. Schermelleh, and I. M. Dobbie, "Assessing resolution in super-resolution imaging," *Methods*, vol. 88, pp. 3–10, 2015.
[30] R. Al Hadi *et al.*, "A 1 k-pixel video camera for 0.7–1.1 terahertz imaging applications in 65-nm CMOS," *IEEE J. Solid-State Circuits*, vol. 47, no. 12, pp. 2999–3012, 2012.
[31] R. Zatta, V. S. Jagtap, J. Grzyb, and U. R. Pfeiffer, "CMOS THz Camera Used as Compact Antenna Test Range," in *Proc. Int. Worksh. Mob. Terahertz Syst.*, 2020, pp. 1–4.

Robin Zatta received the B.Sc. degree in industrial and electrical engineering and the M.Sc. degree in industrial and automotive engineering from the University of Wuppertal, Germany, in 2015 and 2017, respectively. Since 2017, he has been working toward the Ph.D. degree with the Institute for High-Frequency and Communication Technology (IHCT), University of Wuppertal, Wuppertal, Germany, working on novel applications of CMOS THz cameras and SiGe source arrays.

He was a Joint Research Fellow with IHCT, where his research activities included automated experimentation and electromagnetic design during his education. His current research interests include novel applications of CMOS THz cameras and SiGe source arrays and high-frequency analog circuit design in integrated silicon process technologies.

© 2021 IEEE. Personal use is permitted, but republication/redistribution requires IEEE permission. See https://www.ieee.org/publications/rights/index.html for more information.

This article has been accepted for publication in IEEE Transactions on Terahertz Science and Technology. This is the author's version which has not been fully edited and content may change prior to final publication. Citation information: DOI 10.1109/TTHZ.2021.3088278

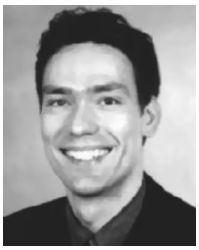

Ullrich R. Pfeiffer (Fellow, IEEE) received the Diploma in physics and the Ph.D. degree in physics from the University of Heidelberg, Heidelberg, Germany, in 1996 and 1999 respectively.

In 1997, he worked as a Research Fellow with the Rutherford Appleton Laboratory, Oxfordshire, England. From 1999–2001, he was working as a Postdoctoral Researcher with the University of Heidelberg on real-time electronics for particle physics experiments at the European Organization for Nuclear Research (CERN), Switzerland. From 2001–2006, he was with the IBM T.J. Watson Research Center, where his research involved RF circuit design, power amplifier design at 60 and 77 GHz, high-frequency modeling, and packaging for millimeter-wave communication systems. In 2007, he received a European Young Investigator Award and led the THz electronics group at the Institute of High-Frequency and Quantum Electronics, University of Siegen, Germany. Since 2008, he holds the High-frequency and Communication Technology chair, University of Wuppertal, Wuppertal, Germany. His current research includes silicon RFICs for mmWave/THz communication, radar, and imaging systems.

Prof. Pfeiffer was the co-recipient of the 2004 and 2006 Lewis Winner Award for Outstanding Paper at the IEEE International Solid-State Circuit Conference, the co-recipient of the 2006 IBM Pat Goldberg Memorial Best Paper Award, the 2008 EuMIC Best Paper Award, the 2010 EuMC Microwave Prize, the 2014 EuCAP Best Paper Award, and the 2017 Microwave Prize, the 2012 and 2018 Jan Van Vessem Award for Outstanding European Paper at the IEEE International Solid-State Circuit Conference. He has been a Distinguished Lecturer for the IEEE Solid-State Circuits Society and the President of the German Association for Electrical Engineering and Information Technology e.V. (FTEI).

© 2021 IEEE. Personal use is permitted, but republication/redistribution requires IEEE permission. See https://www.ieee.org/publications/rights/index.html for more information.